Process window development of DED-LB/M process with coaxial wire for stainless steel AISI 316L

INDERSCIENCE PUBLISHERS
Linking academia, business and industry through research

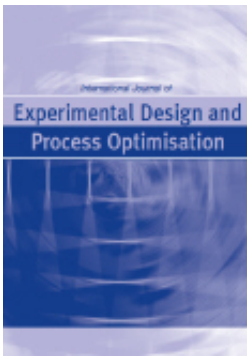

International Journal of Experimental Design and Process Optimisation

ISSN online: 2040-2260 - ISSN print: 2040-2252
https://www.inderscience.com/ijedpo

Process window development of DED-LB/M process with coaxial wire for stainless steel AISI 316L

Panagiotis Stavropoulos, Harry Bikas, Konstantinos Tzimanis, Nikos Porevopoulos, Adriano Nicola Pilagatti, Eleonora Atzeni, Luca Iuliano, Alessandro Salmi

DOI: 10.1504/IJEDPO.2024.10063465

Article History:

Received:	28 September 2023
Last revised:	01 December 2023
Accepted:	01 January 2024
Published online:	29 April 2024

Process window development of DED-LB/M process with coaxial wire for stainless steel AISI 316L

Panagiotis Stavropoulos*, Harry Bikas, Konstantinos Tzimanis and Nikos Porevopoulos

Laboratory for Manufacturing Systems and Automation,
Department of Mechanical Engineering and Aeronautics,
University of Patras,
Rion, 26504 Patras, Greece
Email: pstavr@lms.mech.upatras.gr
Email: bikas@lms.mech.upatras.gr
Email: tzimanis@lms.mech.upatras.gr
Email: porevopoulos@lms.mech.upatras.gr
*Corresponding author

Adriano Nicola Pilagatti, Eleonora Atzeni, Luca Iuliano and Alessandro Salmi

Department of Management and Production Engineering,
Politecnico di Torino,
Corso Duca degli Abruzzi 24, 10129 Torino, Italy
Email: adriano.pilagatti@polito.it
Email: eleonora.atzeni@polito.it
Email: luca.iuliano@polito.it
Email: alessandro.salmi@polito.it

Abstract: This work is focused on the development of a process window for the laser-based directed energy deposition additive manufacturing (AM) process with coaxial wire as feedstock (DED-LB/M) as well as on the investigation of the significance of process parameters on the bead dimensions. This study employs a dual-pronged experimental approach: a one-factor-at-a-time (OFAT) evaluation for qualitative analysis of track dimensions and delineation of the process window, coupled with a full factorial design to derive response surfaces for AISI 316L stainless steel. The aim of this work is to identify the appropriate process parameters by examining the width, height and depth dimensions of the bead and the generation of process related knowledge so as to be used in further experimental work and for process control.

Keywords: directed energy deposition; DED; additive manufacturing; laser-based process; coaxial wire; bead dimensions; design of experiment; AISI 316L; process knowledge; process control.

Reference to this paper should be made as follows: Stavropoulos, P., Bikas, H., Tzimanis, K., Porevopoulos, N., Pilagatti, A.N., Atzeni, E., Iuliano, L. and Salmi, A. (2024) 'Process window development of DED-LB/M process with coaxial wire for stainless steel AISI 316L', *Int. J. Experimental Design and Process Optimisation*, Vol. 7, No. 3, pp.1–26.

Biographical notes: Panagiotis Stavropoulos is an Associate Professor and the Head of Manufacturing Processes Modelling and Energy Efficiency, in the Laboratory for Manufacturing Systems and Automation, Department of Mechanical Engineering and Aeronautics at the University of Patras. His main research interests are focused in the field of conventional, non-conventional and micro-manufacturing processes. He holds a BEng in Mechanical Engineering and an MSc in Advanced Mechanical Engineering from the University of Sussex, UK, PhD in Engineering from the Department of Mechanical Engineering and Aeronautics, University of Patras, Greece, and MBA from the HoU, Greece.

Harry Bikas has been a Research Engineer at the Laboratory for Manufacturing Systems and Automation at University of Patras since 2011. He holds a BEng in Mechanical Engineering and PhD in Engineering from the Department of Mechanical Engineering and Aeronautics, University of Patras, Greece, and an MBA from the HoU, Greece. His main research field is related to additive manufacturing, laser-based processes and machining while he is also working in the area of teaching and learning factories, being close to the academia and industry.

Konstantinos Tzimanis holds a Beng in Mechanical Engineering and an MSc in Advanced Mechanical Engineering and Manufacturing processes from the Department of Mechanical Engineering and Aeronautics, University of Patras, Greece. He is a PhD candidate focusing on Additive Manufacturing area, including process understanding and optimisation as well as process modelling. His other research interests are related to laser based processes and machining under the context of hybrid manufacturing.

Nikos Porevopoulos is a student in the Department of Mechanical Engineering and Aeronautics, University of Patras, Greece. He has been a Research Engineer at the Laboratory for Manufacturing Systems and Automation at University of Patras since 2020 with main research interests around the area of additive manufacturing processes, design for additive manufacturing (topology optimisation) machining and CAx software (CAM, CAD). He has been involved in European funded research project in the Additive Manufacturing context including the provision of services to SMEs for industrial uptake of AM.

Adriano Nicola Pilagatti is currently in his third year of doctoral studies at the Politecnico di Torino, has a diverse academic background, from structural mechanical engineering to optimisation methods. His research employs statistical methods to enhance industrial experiments, primarily focusing on directed energy deposition within the scope of additive manufacturing. An active pursuit of process and product improvement and optimisation characterises his work. He was recognised in 2022 with an award from the euspen talent programme, an esteemed competition uniting elite doctoral students across Europe in physics, mathematics, and engineering.

Eleonora Atzeni is a Full Professor of Technologies and Manufacturing Systems at the Politecnico di Torino. She is a Teaching Professor at the BSc and MSc in Mechanical Engineering, as well as MSc in Automotive Engineering. Her main field of activity is related to additive manufacturing evaluation of mechanical and dimensional performances of additive parts, design for additive manufacturing integrated with economic aspects, application of additive manufacturing techniques, especially for metals. In the field of the above described study and research, she has participated in and spoken at numerous congresses and study meetings.

Luca Iuliano is a Full Professor of Technologies and Manufacturing Systems at Politecnico di Torino, Italy. He is a Teaching Professor at the BSc and MSc in Mechanical Engineering, as well as PhD in Production and Management Engineering. He serves as the Director of the IAM@PoliTo Center and Chairman of the Competence Center (CIM 4.0). His research delves into high-speed machining of Ni-based superalloys, reverse engineering, additive manufacturing, and rapid manufacturing. He authored two Italian books on AM and investment casting and has over 70 publications in academic journals and conferences.

Alessandro Salmi is an Associate Professor of Technologies and Manufacturing Systems at the Politecnico di Torino, Italy and a member of the Advanced Manufacturing Technology (AMTech) research group at the Interdepartmental Integrated Additive Manufacturing Centre at the POLITO. He is a Teaching Professor for the MSc in Mechanical Engineering, MSc in Automotive Engineering and BSc in Design and Communication. His main research topics are related to additive manufacturing technologies and numerical modelling of manufacturing processes.

1 Introduction

Leveraging metal additive manufacturing (AM) is being pursued by various industrial sectors, including energy sector, naval, aeronautical, automotive and offshore industries, etc. (Stavropoulos, 2023). According to Wohlers Report (2023), an overall worldwide growth in AM products and services of 18.3% is noticed, continuing a trend of double-digit AM industry revenue growth for the last 20 years. On top of that, AM market has been growing at an increasing rate in recent years since the processes have become more reliable and with improved productivity rates (Wohlers et al., 2019). The key barrier for a greater adoption is identified on the limited on line control due to poor process understanding and complex physics behind it (Chen et al., 2022; Sofia and Ethiraj, 2020; Rey et al., 2022). Significant research has been directed towards developing advanced quality process monitoring devices. The latter are intended to provide high-fidelity data for models that can address the complexities of the physics involved and enhance the understanding of the process (Stavropoulos, 2022; Panza et al., 2022). Towards this direction, significant research is made also on the correlation of process variables and defects by studying process data so as to provide defect free parts (Rey et al., 2022), contributing to zero-defect manufacturing and reduced consumption of resources being in line with the green deal requirements (Stavropoulos, 2022;

Panagiotopoulou et al., 2023a, 2023b). Using AM for repair and remanufacturing processes (Stavropoulos and Panagiotopoulou, 2022), the environmental footprint and the dismiss costs can be further reduced increasing its attractiveness to industry (Stavropoulos et al., 2020, 2018; Panagiotopoulou et al., 2023b; Piscopo and Iuliano, 2022; Steinhilper, 1998).

Among the AM processes, directed energy deposition (DED) processes provide high productivity rates as well as end parts of high quality, structural and surface, being appropriate for industrial applications. Wire fed DED such as laser based DED (DED-LB/M) and wire arc additive manufacturing (WAAM) provide improved structural performance due to less intrinsic defects and high productivity due to high deposition rate (Bikas et al., 2016) compared to powder bed processes.

This work is focused on the wire DED-LB/M process for AISI 316L material, which combines the fine surface quality due laser beam as heat source compared to wire arc in WAAM and the improved deposition rate compared to powder DED-LB/M. Additionally, wire feedstock is 3 to 5 times less expensive than the same material powder. It also offers enhanced efficiency in material utilisation, especially compared to powder DED. Powder particles can scatter in the melt pool, sometimes remaining non-melted on the part surface or in the substrate. Approximately 25% of the powder can be lost if not properly recovered and reused (Pilagatti et al., 2023). A stable process hinges on maintaining a consistent melt pool, which, in turn, requires the interaction between the wire and lasers to be uniformly distanced above the substrate. Achieving this consistency is a complex challenge, as factors like heat accumulation, layer height, and laser calibration can compromise process stability (Stavropoulos and Foteinopoulos, 2018). These factors affect the area where the wire-substrate is being hit by the lasers and as such as they influence the uniform heat of wire tip and the layer below. Figure 1, demonstrates this effect. Heat accumulation results in excessive re-melting of the previously printed layers, leading to a shrinkage that increase the distance between the deposition head and the part as well as in a wavy top layer due to the extreme heat on the provided material. The same is also happening when the layer height is smaller than expected. With increasing number of layers, the stand-off distance increases, and material droplets are expected. The stiffness of wire and the consistent size across the motion, compared to the powder particles that follow off axis configuration with a varying size across the motion, leads to non-stable processes when less standoff distance is achieved due to wire oscillation on the surface. Focused experimental work is necessary to provide the required process understanding that links the process variables to the process responses.

The current research involves a multiple geometrical responses assessment through a full factorial design to predict the geometric characteristics of single tracks created by the wire DED-LB/M system. The focus of the study is on geometric features such as width (W), height (H), and depth (D), which are used in calculating the specific ratios of single tracks, such as W/H and H/D. According to literature these two ratios are used as ‘Go’ – ‘No Go’ conditions for the decision making regarding the appropriate parameters for the process. If the calculated ratios are below or above the indicated values, inadequate bonding between the tracks and the substrate is expected (Jiayun et al., 2021; Wang and Kashaev, 2022).

This study stems from the outcomes obtained while examining the boundaries of the process parameters and progresses towards developing a comprehensive design of experiments (DoE) capable of capturing the non-linearity of the process. A total of 27 deposited tracks, each extending up to 10 cm, were sectioned to facilitate a chemical etching process, followed by analysis and measurements using an optical microscope. The data gathered were processed through the commercial statistical software Minitab 20.1.3. Specifically, analysis of variance (ANOVA) in conjunction with the standard stepwise regression method that was employed to derive the reduced model containing only significant terms. Lastly, exploiting the response surface methodology (RSM), the response against the active factors was plotted and examined.

2 System characterisation

The work has been conducted by using a DED-LB/M wire head produced by Meltio (Linares, SPA), integrated on a robotic arm by Yaskawa (Kitakyūshū, Fukuoka, JPN). The head consists of six off axis fibre lasers (976 nm) and a co-axial wire. Each one of the lasers reaches 200 W and in total the system can deliver 1,200 W while the laser spot diameter is 0.4 mm. The fed wire can range between 0.8 mm and 1.2 mm. The build plate was a 10 mm thick AISI 304 plate and the selected diameter for the AISI 316L wire was $(1.00 \pm 0.01)^1$ mm. The consistency of diameter has been validated and it is around the given tolerance of manufacturer while metallurgical analysis has not been performed neither to substrate nor to the wire, since this is part of a following work where the effect of process thermal phenomena are studied on how they affect the microstructure of the part and as such it will be interesting to identify the microstructure of the raw material and compare it with the end part. For the experiments the distance between the head and the substrate (stand-off distance) was kept constant at 6 mm following the recommendation of machine manufacturer, otherwise, excessive balling is expected or over-melt of the substrate (Figure 1). The inert gas (Argon) flow was kept constant at 8 $L \cdot min^{-1}$, being provided via the gas nozzle to the melt pool.

Figure 1 Distance between deposition head and substrate (stand-off distance), (a) wire unmelt, (b) correct melting, (c) wire pre-melting (see online version for colours)

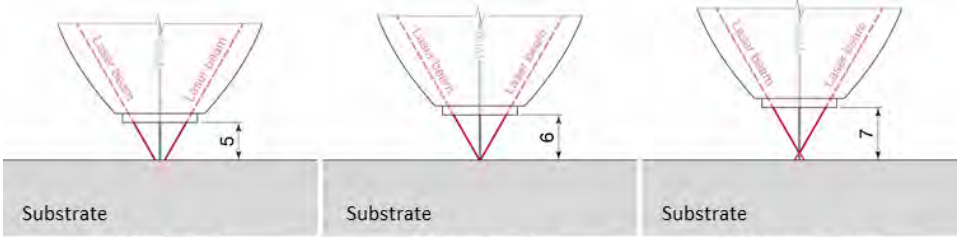

(a) (b) (c)

The system is depicted in Figure 2.

Figure 2 DED-LB/M system with coaxial wire and off axis fibre lasers (see online version for colours)

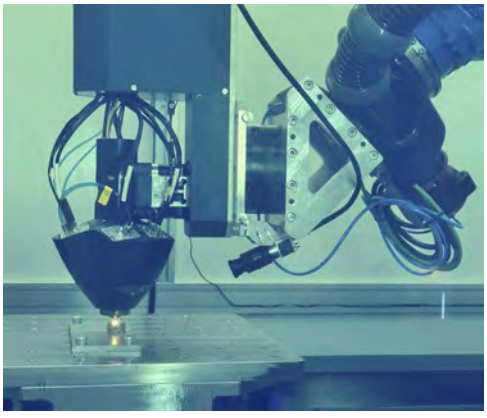

3 Methodology

The aim is to extract the process window for a new material/machine with a limited number of experiments. The authors used both a one-factor-at-a-time (OFAT) approach and the factorial design to study how process variables influence process mechanisms, focusing on track dimensions. Key performance indicators (KPIs) for the process, like speed and energy efficiency, and for the part, such as surface quality, distortion, and structural integrity, are affected by these process inputs depicting their significance on the process (Bikas et al., 2016; Stavropoulos et al., 2023a, 2023b). This highlights the importance of understanding the impact of process parameters on the KPIs.

Although these KPIs refer mainly to functional parts and complex geometries, this methodology considers simple, single lines as the first step for the experimental work, conserving resources while also facilitating the evaluation of the end parts by performing measurements with microscope on polished bead sections. *W*, *D* and *H* dimensions are obtained through an optical microscope so as to identify which set of parameters produces beads within the *H*/*D* and *W*/*H* limits. Empirically, regardless the material, *W*/*H* should be between 2.5 and 3.5, and *H*/*D* between 1.0 and 1.5 to have adequate bonding of the deposited material to the substrate (Jiayun et al., 2021; Wang and Kashaev, 2022). The experimental work considers the recommendation of the machine manufacturer as starting point, ensuring that the provided energy will be capable to melt the substrate and the fed material.

Apart from filling a longer list of appropriate process parameters for the studied material, the scope of the experimental work is to understand also the influence of process parameters on the studied dimensions. By transforming these outputs to knowledge, it can be used in more complex designs aiming to ensure stable and high-quality processes. Common issues that need to be tackled in wire DED-LB/M process is the collision of fed material to the substrate due to over-deposition issue as well as the balling that can be caused due to under-deposition and therefore longer distance between the head and the substrate. Under deposition is related to the heat accumulation and continuous re-melting of material, achieving less height than expected

in a specific number of layers or due to wrong calculation of layer height. As such balling is expected (lasers hit the wire above the substrate surface), leading to unstable process and failed part (Figure 3). When this issue is detected, more material is fed to the system by increasing only the wire feed rate (WFR). On the other hand, when over-deposition is detected the WFR reduces. Another issue is the overheat of the system in thin wall structures when the input power remains constant across the height since the new material is deposited in an already hot surface. This information is used so as to drop the power levels when the heat accumulation in the system has reached an equilibrium, and such as drop of power value is suggested to avoid excessive heat in the system and re-melting or keyholes. By reducing the power when the stored heat remains constant, the width remains stable. To support this argument, the link of laser power to the width needs to be investigated in the simple, single line case.

This process understanding begins with the single tracks that aim to provide the correlation of process parameters to *W*, *H*, *D* which leads to the calculation of layer height for multi-layer parts as well as the calculation of the overlap dimensions and the definition of the number of walls that are needed to achieve a desired width. Figure 4 introduces the critical dimensions *W*, *H*, *D* in a section of the single track.

Figure 3 Process stability monitoring with off axis melt pool camera, (a) balling, (b) wire buckling and overdeposition, (c) stable deposition

(a) (b) (c)

Figure 4 Geometrical features of the melt pool; depth (*D*), width (*W*), height (*H*)

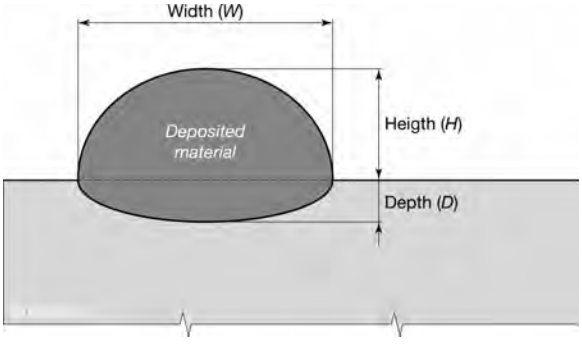

Source: Image adapted from Piscopo et al. (2019)

These single tracks have been developed around a specific *E*, so as to ensure stable process and consistent dimensions across the track [Figure 5(b)], otherwise no meaningful outputs can be extracted [Figure 5(a)]. The linear energy density

demonstrates the required energy to narrowly melt the provided material, which is the information that is needed in single tracks development. When multi-layer or overlapping tracks are developed, the energy per volume and the energy per surface can be calculated and used as an additional process variable. During the full factorial design, process stability is not a prerequisite. The behaviour of the system is explored within set limits, and unstable deposition is anticipated.

In Figure 6, the steps for the extraction of the critical dimensions from the single tracks are depicted. The build plates are labelled with permanent marks and then are cut in sections (two sections per track), to investigate the *W*, *H*, *D*. After these cuts, the cross sections are polished with sandpapers and then cleaned with a polishing paste. For AISI 316L, sandpapers from P200 to P2000 have been used gradually to make the surface shiny. Then, hydrochloric acid is used as etchant, distinguishing the molten material and the substrate (Frederick et al., 1976). A ISM-DL301 optical microscope by Insize (Derio, SPA) was used to measure the track geometry features [Figure 6(d)]. The human error during these measurements is 10%, being transformed as 0.05 mm in depth and 0.1 mm in height and width dimensions. In case that a set of parameters have been accepted due to this kind of error, it will be rejected in later stages of process window development workflow when the bonding between layers will be examined with structural strength experiments and computed tomography (CT) scan for the identification of cracks/porous. On top of that, these errors are accumulated during multi wall and overlapping structures, affecting the calculation of layer height and the hatching distance, leading to non-stable processes. This finding points out the significance of process monitoring and process control, where the material feed and the laser power could be modified in the process to maintain a stable process.

Figure 5 Experimental work based on stable process to extract bead dimensions, (a) non-stable deposition, (b) stable deposition (see online version for colours)

(a) (b)

Finally, among the process parameters of wire DED-LB/M process only the laser power, the robot speed and the WFR will be investigated for the development of the process window. The standoff distance (Figure 1) is a fixed value according to the machine manufacturer, depicting the significance of hitting in the correct area the wire and at the same time the substrate, while the inert gas flow relies also on the suggestion of machine manufacturer for a specific material. The latter parameter could affect the quality of the bead being linked to corrosion. Finally, parameters such as substrate temperature,

deposition orientation, etc. can be linked more to the structural performance of multi wall and solid parts. Finally, the parameters have been divided as process related and part related parameters. Laser power, WFR and robot speed can affect the stability of a process even for single tracks, while the rest of parameters can be decided carefully and adjusted based on the specifications and the geometry of the under development part.

Figure 6 Extraction of *W*, *H*, *D*, dimensions, (a) single tracks, (b) sections to be polished, (c) etching with hydrochloric acid, (d) measurements with microscope (see online version for colours)

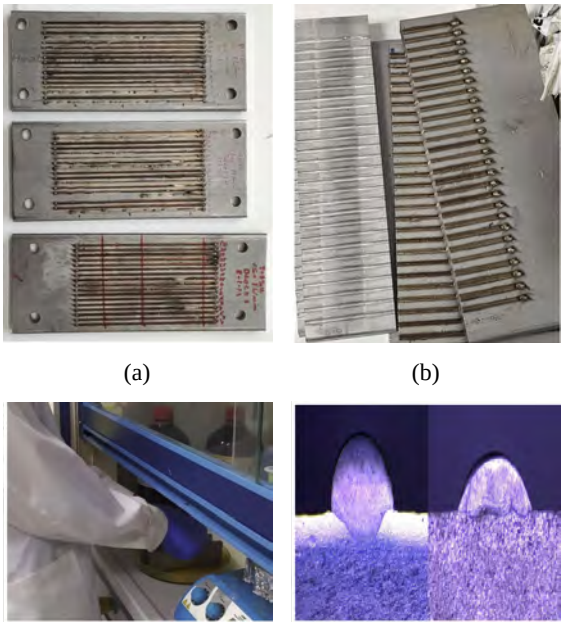

(a) (b)

(c) (d)

4 Preliminary exploration of parameters through OFAT approach

Given a new and entirely unfamiliar wire DED-LB/M system, it is deemed necessary to investigate the system starting with the process parameters recommended by the system manufacturer, with small incremental steps to explore the unknown regions of the process parameters and how these influence the process and product KPIs. Since some of the process variables may differ on the various systems (number of lasers, laser beam diameter, dimensions of build plate, specifications of raw material) the given parameters work as an indicator about the linear energy density E that favours the process stability for a given material. E is the ratio of laser power (P) over the robot scan speed (v).

Although inefficient from an experimental standpoint, the OFAT approach becomes indispensable, given the novelty of the system and the inherent instability and complexity of the process. On top of that OFAT outputs can be used to understand the effect of process parameters on dimensions not only in single tracks but also in every design, since an insight is provided about their effect on dimensions and at the same time on processes stability. Compared to the DED processes with powder, in wire feed systems, the as

expected height growth is a requirement, otherwise there is either a collision of the wire on the melt pool or the balling phenomenon which lead to unstable and failed processes (Zuo et al., 2022) as presented in Section 3. Therefore, the knowledge of the influence of process parameters on the track height and the understanding of how to maintain constant growth are expected outcomes of the work that begins with the single tracks and the OFAT approach. Section 4 elucidates the impact of process variables on track dimensions. Subsequently, Section 5 provides a structured experimental workflow, delineating the process window and pinpointing the optimal parameters within the constraints of the machine and the evaluated window.

Therefore, this initial exploration aims to discern step by step the potentials, limitations, and operating windows of the wire DED-LB/M process, given a specific system. This investigation comprises three successive steps, each involving fixing one or more factors and exploration in steps with three replications (contravening the randomisation principle) to determine the stability of the process. Given that a factorial design is not being utilised in this initial phase, the responses of interest are the typical geometric characteristics of the single tracks, specifically *W*, *H*, and *D*. This becomes necessary as the use of the OFAT approach would not adequately describe complex responses such as ratios, considering the complexity of the physical phenomena involved. On top of that, the knowledge of how each factor affects the bead dimensions is necessary during the implementation of control strategies, when phenomena such as over-deposition/under-deposition and heat accumulation must be addressed. For the available robotised wire DED-LB/M system, the machine manufacturer suggests the *E* to be around to 75 J·m^{-1} for stainless steel AISI 316L. At the same time, the WFR varies so as the ratio of v over WFR, denoted as (*v*/WFR), must be close to 1. The exploratory analysis was conducted to assess the significance of each parameter on the bead dimensions and to define a process window where the process is stable around a *E* for a given material.

4.1 Investigation on the WFR

In this exploratory phase, the focus was directed towards the WFR. The *E* was maintained at a constant value of 73 J·mm^{-1} by setting *P* = 800 W and *v* = 11 mm·s^{-1}. The exploration of the WFR began from a starting point of 7 mm·s^{-1}, incrementing by 1 mm·s^{-1} each step until the rate of 13 mm·s^{-1} was attained (see Table 1) for a total of 21 tracks divided among seven factor levels with three replications each.

Table 1 Experiment design for WFR factor at *E* = 73 J·mm^{-1} (*P* = 800 W; *v* = 11 mm·s^{-1})

WFR/(mm·s^{-1})	*v/WFR*
7	1.6
8	1.4
9	1.2
10	1.1
11	1.0
12	0.9
13	0.8

The results of measurement of the geometrical features of the tracks, namely *W*, *H*, and *D*, were analysed using a one-way ANOVA assuming unequal variance across levels. The ANOVA (see Table 2), which tests for equality among levels, returned that WFR is highly significant only for the response *H* (p-value lower than 0.1%), indicating that at least one of the WFR levels affects the response and, therefore *H* will be the only feature considered for the next step of this stage.

Table 2 ANOVA for *H*/mm

Source	*df*	*Contribution/%*	*Adj. SS*	*Adj. MS*	*F*	*p-value/%*
WFR	6	97.61	0.210692	0.035115	95.32	< 0.1
Error	14	2.39	0.005157	0.000368		
Total	20	100				

The regression model returned a standard deviation of residuals (*S*) of 0.012, an R^2(adj.) of 98%, and a R^2(pred.) of 97%, all of which are satisfactory. Examining the residuals of the model reveals no significant issues, except for slightly decreasing variability in the versus fits plot. Moreover, based on the lack-of-fit test, the obtained model appears adequate, as the p-value is higher than the significance level of 5%. This indicates that the difference between the predicted values and the observed data is not statistically significant. Therefore, it can be concluded that the model is a good fit for the dataset being analysed and the equation is as follows:

$$H = 0.0008 + 0.04987 \cdot WFR$$

As evidenced by Figure 7, an increase in the material supplied to the melt pool, while keeping other factors constant, increases the *H* of the track.

Figure 7 *H* versus WFR regression model (see online version for colours)

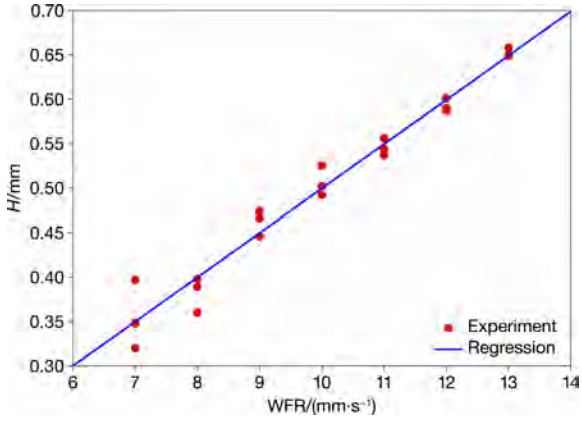

This outcome is quite intuitive, yet it should be noted that this statement is valid only within the chosen levels of *P* and *v*. With the recommended values of parameters, a 0.5 mm height is achieved, with a maximum variation by around 30% at the limits of the investigated range (Akritas and Papadatos, 2004; Minitab, 2023a). This range is more than 10% increase which is considered as a reasonable experimental error during the measurements on microscope (Stavropoulos et al., 2022).

4.2 Investigation on laser power keeping constant the specific energy and the deposition ratio

In the subsequent experimentation, a distinct approach was employed. It becomes more instructive to assess whether, alongside *E*, one of its two parameters, *P* and *v*, significantly influences the variation in track geometries. Therefore, to appreciate a qualitative change in *E*, it was chosen to analyse the *P* values since they have a wider range compared to *v*. This implies that the same *E* is being analysed at different *P* levels. Moreover, unlike the first experiment, there is a change in the material volume delivered to the melt pool by maintaining the *v*/WFR ratio constant. Here, the *E* was kept constant at 73 J·mm^{-1}, and *P* increased from 650 W to 950 W, leading to a corresponding increase in the speed of the deposition head. Additionally, the deposition ratio between *v*/WFR was maintained constant at 1.1. The parameters utilised in this experiment are outlined in Table 3, and three replication was performed at each level.

Table 3 Experiment design for *P* factor at *E* = 73 J·mm^{-1} and *v*/WFR = 1.1

P/W	*v/(mm·s^{-1})*	*WFR/(mm·s^{-1})*
650	8.9	8.1
700	9.6	8.7
750	10.3	9.4
800	11.0	10.0
850	11.7	10.6
900	12.4	11.3
950	13.1	11.9

At this stage of the experimentation, results analysis becomes more complex due to the deliberate constant ratios of some factor ratios. ANOVA was assessed both on main effects and higher order terms utilising a standard stepwise method with alpha-to-enter and alpha-to-remove thresholds set at 10% to include only significant factors, hence accommodating terms near the 5% significance level. Stepwise regression is an iterative statistical technique utilised to systematically select influential predictor variables, thereby facilitating model reduction. By leveraging partial F-tests, it sequentially adds or removes variables, thereby enhancing the precision of the final model and enabling more robust predictions, all while maintaining the parsimony and interpretability of the model (Montgomery and Runger, 2020; Minitab, 2023b). The results obtained in this phase broaden the knowledge acquired from the previous experiment, as the exploration of the process windows and the aim are different. *P* is significant for all the responses, namely *W*, *H* and *D*. All obtained regression models are linear, do not exhibit any major issues with residuals, and have satisfactory *S*, R^2(adj.), and R^2(pred.). The summarised results are presented in Table 4. These findings highlight the complex interactions between the process parameters and their impact on the geometric characteristics of the tracks.

The regressions shown in Figure 8(a) elucidate that an increase in *P* leads to a wider *W*, a decrease in *H* and an increase in *D*. It can be seen that *P* has a strongest influence on the *W*, compared to other two responses. This statement is elaborated in Section 4.3. The authors find it useful to highlight the trends in geometric characteristics of the tracks with the ratios *H*/*D* and *W*/*H* in Figure 8(b). This approach facilitates a comprehensive

understanding of the complex interactions between the parameters and their resultant effects on the track geometry.

Table 4 Regression analysis

Resp.	*S*	R^2*(adj)/%*	R^2*(pred)/%*	*Regression equation*
W	0.034	89	86	$W = 1.0810 + 0.000875 \cdot P$
H	0.017	57	47	$H = 0.6777 - 0.000195 \cdot P$
D	0.019	72	67	$D = -0.1500 + 0.000314 \cdot P$

These trends can be better understood from a physical perspective. An increase in *P* generally leads to enhanced heat transfer, elevated localised temperatures, and thermal gradients. These factors, in conjunction with the relatively low thermal diffusivity inherent to the substrate material (AISI 304), could affect the rate of change in temperature over time in the melt pool area, potentially by orders of magnitude (Mazzarisi et al., 2020; Mustafa et al., 2014). In the experiment, the *E* was kept constant, implying that the percentage increase in v equals the one of the *P*. However, the net variation in speed is not so high to counteract the thermal effect of the laser, which remains the main factor influencing melt pool generation. This can be justified considering that in DED, the material is fed continuously, requiring some time to stabilise the melt pool, in the range of 10^{-3} s and then move (Stavropoulos et al., 2022). As such, lower speeds are achieved compared to powder bed processes.

Figure 8 (a) Regression plots and (b) *W*/*H* and *H*/*D* plots (see online version for colours)

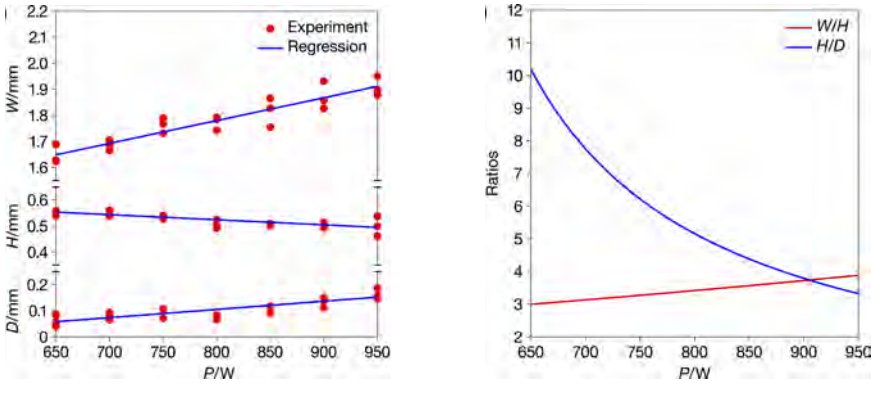

(a) (b)

With an increase in *P*, the *W* expands and the *D* increases, with a more significant impact on *D* due to the heat losses through convection and radiation that are imposed on *W* and *H*, while *D* is affected mostly from conduction. Subsequently, when *W* increases, *H* decreases accordingly, as the track cross-section is constrained by the material feed, specifically by the ratio between *v* and WFR. However, it should be emphasised that while these findings provide crucial insights into the thermal dynamics at play, they primarily offer a qualitative understanding and diverge from the primary focus of this investigation. This finding is of utmost importance, suggesting that the *E* does not hold the same significance at different levels of *P*; thus, it has limited usefulness in describing

the phenomenon that occurs during the deposition of single tracks and in predicting the direction of change for the single tracks dimensions.

4.3 Investigation on laser power keeping constant the travel speed and the deposition ratio

The third and final investigation was conducted based on the results of the two previous experiments, focusing on *P* and increasing values of *E*. In this scenario, the values for *v* and WFR were kept constant at 11 mm·s^{-1} and 10 mm·s^{-1}, respectively, yielding a constant *v*/WFR ratio of 1.1. Six unbalanced levels of *P* were investigated as reported in Table 5, with three replications for each. Thus, a one-way ANOVA provides the correct analysis in this case.

Table 5 Experiment design for *P* factor, at *v* = 11 mm·s^{-1} and *v*/WFR = 1.1

P/W	*E/(J·min^{-1})*
700	63.6
800	72.7
850	77.3
900	81.8
950	86.4
1,000	90.0

Table 6 Regression analysis

Resp.	*S*	*R^2(adj)/%*	*R^2(pred)/%*	*Regression equation*
W	0.036	91	89	$W = 0.893 + 0.001134 \cdot P$
H	0.015	79	73	$H = 0.7091 - 0.000242 \cdot P$
D	0.026	53	47	$D = -0.1363 + 0.000284 \cdot P$

Figure 9 (a) Regression plots and (b) *W*/*H* and *H*/*D* plot (see online version for colours)

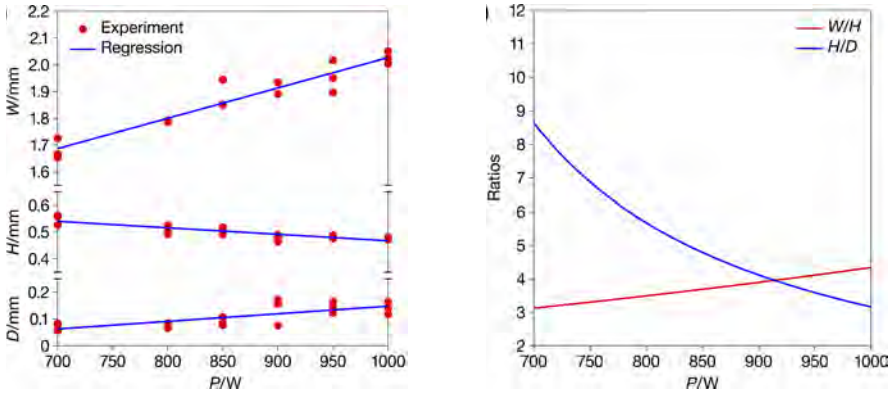

(a) (b)

As expected from previous section, the results indicate that *P* is significant for all three geometric characteristics of the tracks and, consequently, for the ratios. A regression

analysis was performed, and the results are acceptable only for *W* and *H* but almost acceptable for *D*, as it has a fairly low R^2(adj.) value. The latter means the model explains approximately 50% of the data variability. Although *D* could be fitted with higher-order polynomial models, the marginal improvement in the R^2(adj.) does not justify the increased model complexity. Hence, following Occam's razor principle, a simpler and more parsimonious model is preferred (Domingos, 1999); however, this digresses from the aim of this study at this stage. The responses for all the geometric features are summarised in Table 6, while the ratios of the interpolations are depicted in Figure 9(a).

It is noteworthy that, despite the differences in the experimental aims and values between this study and the second experiment discussed in Section 4.2, the trends observed in the regression analyses are strikingly similar. This comparison suggests that the influence of *P* on geometric features is not sensitive to variations in other process parameters. Finally, the ratios *W*/*H* and *H*/*D* are plotted in Figure 9(b). As observed, with an increase in *P*, there is a slight increase in *W*/*H*. Similar to the second experiment; this indicates an increase in track width and a decrease in height. Conversely, *H*/*D* decreases dramatically, suggesting enhanced track dilution into the substrate. Having completed the evaluation of the three successive experimental workflows, the qualitative outputs can be used in more complex shapes (single walls, single layers, multi wall and solid parts), where it is necessary to modify the values of process parameters online to maintain stable process and constant growth. The key outcomes are:

- When all other parameters and the linear energy density are held constant, a change in *P* directly affects *W*. Specifically, increasing *P* leads to an increase in *W*, primarily due to the additional heat introduced into the system;
- With constant all the other parameters, the change of WFR affects directly the *H*. By increasing the WFR, the *H* increases. Although the W is also affected with the same way, the increase in *H* is significantly larger;
- Although E and the term *v*/WFR remain constant by changing simultaneously the power and speed, the *W*, *H* change. This conclusion indicates that the values of *P*, *v* and WFR have a strong influence on the bead dimensions. By achieving the same *E* and *v*/WFR, with different combinations of *P*, *v* and WFR respectively the bead dimensions change. Therefore, to understand how the bead dimensions will change, we should keep at least one parameter constant.

5 Factorial design

After delineating the physical limits of the system under study, consulting the machine manufacturer while also studying the physics of the process the region of interest for exploration has been carefully selected. In the following experimental campaign, our responses shifted from geometric dimensions to the ratios of *W*/*H* and *H*/*D* which is the actual target to identify the appropriate values for the process parameters. As it is depicted in Figure 10(a), in order to characterise a set of parameter as appropriate the *D*, should be in accordance to *W*, and *H*, otherwise the bonding between the deposited material and the substrate is weak [Figure 10(b)].

Figure 10 Comparison of single tracks, (a) between thresholds, (b) out of thresholds (see online version for colours)

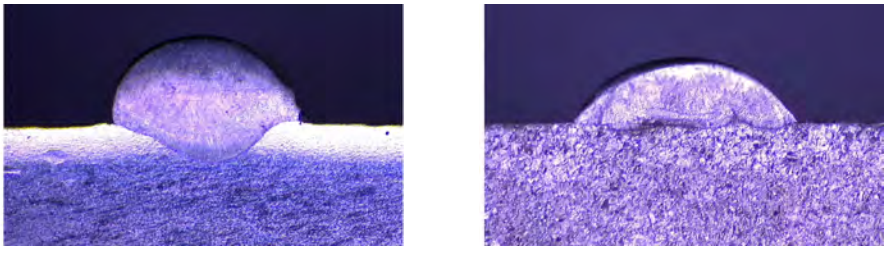

(a) (b)

Given the complexity of the phenomena involved in the process and the nonlinear relationships, as seen in Figure 11, a 2k full factorial design with central point was selected, allowing for the detection and modelling of two-way and three-way interactions and testing if there is a quadratic effect. The levels of the factors explored are summarised in Table 7. Figure 11 elucidates the differences between the OFAT approach, addressed in prior sections, and the full factorial design, which is the focal point of the current section.

Figure 11 Comparison between the first experimental procedure and the factorial approach (see online version for colours)

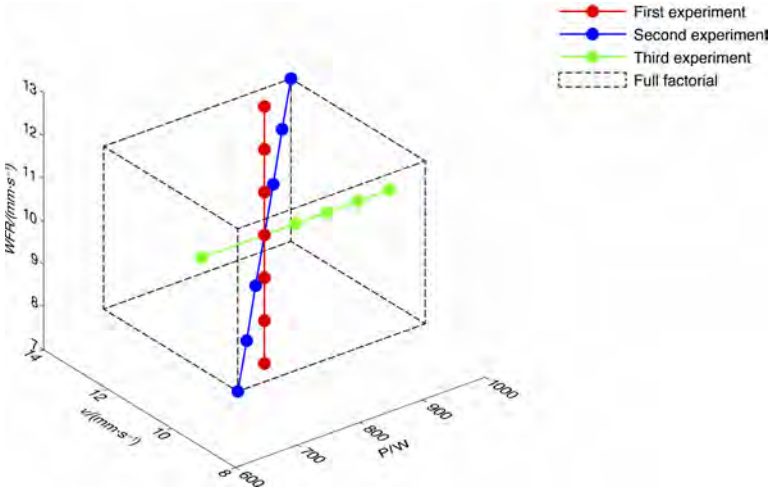

Table 7 Process variables values and centre points used in the planned experimentation

Process variable	*Values*	*Centre point*
P/W	650–950	800
v/(mm·s^{-1})	8.9–11.9	11
WFR/(mm·s^{-1})	8.1–11.9	10

With the substrate capable of accommodating a maximum of 27 tracks, the decision was made to fully exploit this capacity by adopting three replications for both corner and

central points. This approach facilitates the evaluation of a *very large* effect size (Lenth, 2001; Sawilowsky, 2009), offering a power of approximately 80%. Hence, this provides a substantial degree of robustness to the underlying assumptions in this application.

Table 8 Arrangement and measurements of the experimental design

Std. order	*Run order*	*Centre point*	*P/W*	*v/(mm·s^{-1})*	*WFR/(mm·s^{-1})*	*W/H*	*H/D*
1	19	1	650	8.9	8.1	3.134	9.877
2	17	1	950	8.9	8.1	4.752	3.731
3	8	1	650	13.1	8.1	3.120	6.015
4	26	1	950	13.1	8.1	5.640	3.761
5	15	1	650	8.9	11.9	2.244	12.143
6	25	1	950	8.9	11.9	3.093	5.899
7	14	1	650	13.1	11.9	1.857	13.774
8	9	1	950	13.1	11.9	3.565	3.759

Table 8 Arrangement and measurements of the experimental design (continued)

Std. order	*Run order*	*Centre point*	*P/W*	*v/(mm·s^{-1})*	*WFR/(mm·s^{-1})*	*W/H*	*H/D*
9	7	1	650	8.9	8.1	2.912	9.638
10	3	1	950	8.9	8.1	4.570	3.014
11	10	1	650	13.1	8.1	3.629	7.018
12	5	1	950	13.1	8.1	5.848	2.792
13	6	1	650	8.9	11.9	2.521	14.478
14	22	1	950	8.9	11.9	2.903	5.727
15	21	1	650	13.1	11.9	2.382	11.501
16	11	1	950	13.1	11.9	4.301	2.782
17	1	1	650	8.9	8.1	2.910	6.565
18	2	1	950	8.9	8.1	4.505	2.968
19	18	1	650	13.1	8.1	2.856	8.371
20	13	1	950	13.1	8.1	6.073	1.709
21	27	1	650	8.9	11.9	1.424	14.090
22	12	1	950	8.9	11.9	2.975	4.517
23	20	1	650	13.1	11.9	1.325	10.243
24	4	1	950	13.1	11.9	3.700	3.472
25	23	0	800	11.0	10.0	3.894	5.976
26	24	0	800	11.0	10.0	3.415	6.250
27	16	0	800	11.0	10.0	3.628	7.455

The experiment was conducted successfully by the authors in the system that is depicted in Figure 2, with particular attention given to the three principles of industrial experiments, namely replication, randomisation, and blocking. As visible in Table 8, the order in which the tests were conducted was randomised. All tracks were replicated three

times and produced on the same day by the same operator on a rectified substrate with constant surface roughness, thus obviating the need for blocking.

5.1 W/H analysis

The model analysed in this section, defined as the reduced model, is derived from a refined version of the full factorial design inclusive of the curvature and two-way and three-way interactions. This refinement is executed to exclude non-significant terms from the original one to yield a more parsimonious and statistically robust interpretation of the data (Montgomery, 2022). This model was developed using a standard stepwise method with alpha-to-enter and alpha-to-remove set at 10% without imposing a hierarchical model. The reduced model yielded a standard deviation *S* of 0.34, an R^2(adj.) of 93%, which means that the model explains almost 93% of the variability of the data and an R^2(pred.) of 89%, which is an indicator of how well the model could predict new observations. Moreover, test 27 was identified as an outlier by the Grubbs test (Barnett and Lewis, 1994). However, it did not appear crucial in the overall interpretation of the results and was not included in the fitting or elimination process. As illustrated in the Table 9, all three main effects and the interaction between *P* and WFR are significant and therefore included in the model. Significantly, while the derived model does not present any lack-of-fit or curvature, an analysis of the residuals does reveal slight heteroscedasticity in the versus fit plot. Despite this, no pressing concerns remain regarding the overall performance and reliability of the model. Indeed, the hypothesis that the residuals follow a normal distribution cannot be rejected at a significance level of 5%, as confirmed by the Anderson-Darling test (Nelson, 1998). Moreover, no peculiar patterns are observed in the order of residuals, a testament to the effective randomisation process adopted.

Table 9 W/H ANOVA for the reduced model

Source	*df*	*Adj. SS*	*Adj. MS*	*F*	*p-value/%*
Model	5	36.4714	7.2943	61.52	< 0.1
Linear	3	34.1340	11.3780	95.96	< 0.1
P	1	19.4600	19.4600	164.13	< 0.1
v	1	1.6808	1.6808	14.18	0.1
WFR	1	12.9932	12.9932	109.59	< 0.1
2-way interaction	2	2.3374	1.1687	9.86	0.1
P · v	1	1.6563	1.6563	13.97	0.1
P · WFR	1	0.6811	0.6811	5.74	2.6
Error	21	2.4899	0.1186		
Curvature	1	0.1281	0.1218	1.09	31.0
Lack-of-fit	2	0.2436	0.1218	1.04	37.5
Pure error	18	2.1181	0.1177		
Total	26	38.9612			

The authors preferred to express response surface regression coefficients in coded units due to their distinct advantages. These coded design variables in factorial experiments provide clear benefits, including their orthogonality, comparability of effects, and

uniform precision. These characteristics make them a superior choice for conducting reliable and interpretable analyses. The regression equation in coded terms is as follows:

$$W/H = 3.4511 + 0.9005 \cdot P + 0.2646 \cdot v + 0.7358 \cdot WFR + 0.2627 \cdot P \cdot v - 0.1685 \cdot P \cdot WFR$$

Table 10 provides a detailed breakdown of the units of measure, regression coefficients, standard errors of the coefficients, and their statistical significance.

Figure 12 shows the factorial plots for the main effects. Notably, the *W*/*H* ratio increases correspondingly with an increase in both *P* or *v*, with *P* demonstrating a substantially more significant effect than *v*. This trend is also evident from the regression equation, as it is expressed in coded units. Hence, corroborating the second experiment described in Section 4.3, as the level of *P* increases the track has a greater *W* and a smaller *H*. Conversely, from the perspective of WFR, as the material feed into the melt pool increases, the ratio *W*/*H* decreases. This is because *H* increases, in line with the first experiment outlined in Section 4.1.

Table 10 Estimates of W/H parameters of the model in coded units

Variable	*Parameter*	*Coef.*	*SE Coef.*	*p-value/%*
Constant	β_0	3.4511	0.0663	< 0.1
P	β_1	0.9005	0.0703	< 0.1
v	β_2	0.2646	0.0703	0.1
WFR	β_3	0.7358	0.0703	< 0.1
$P \cdot v$	β_{12}	0.2627	0.0703	0.1
P · WFR	β_{13}	–0.1685	0.0703	2.6

Figure 12 *W*/*H* main effects factorial plot (see online version for colours)

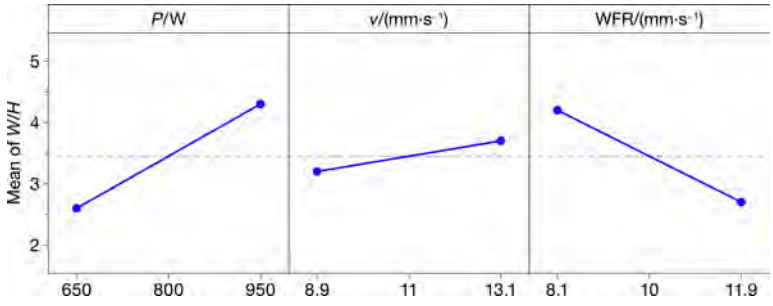

The interaction between *P* and *v* emerges as the most significant among the two interactions included in the model, as depicted in Figure 13 and Table 10. An increase in *P* corresponds to an amplified effect on the response, whereas an escalation in *v* leads to a decrement in the *W*/*H* ratio. This observation is attributable to the increased deposition head speed while maintaining a constant WFR, causing the *v*/WFR ratio to rise and consequently feeding less material into the melt pool. Concerning the two-way interaction between *P* and WFR, it is noteworthy that the influence on the *W*/*H* ratio intensifies as WFR decreases. Specifically, an increase in *P* coupled with a decrease in WFR triggers a higher value in the response. This trend makes intuitive sense as a larger

P broadens the melt pool, and with less material (lower WFR), there is a reduction in *H* growth. Conversely, at lower *P* levels where the melt pool is narrower, the effect of WFR variation is less pronounced.

Figure 13 *W*/*H* interactions plot (see online version for colours)

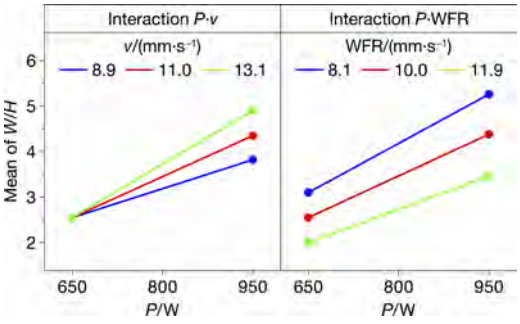

Finally, contour plots were plotted in Figure 14, at the central point. This step was crucial to visualise the surfaces since three factors were involved. One of the three parameters must be fixed to construct a contour plot, while the others can vary. Therefore, for *P* and *v*, WFR was fixed at 10 mm·s^{-1}; for v and WFR, *P* was held constant at 800 W; and finally, for *P* and WFR, *v* was set to 10 mm·s^{-1}.

Figure 14 *W*/*H* contour plots at *P* = 800 W, *v* = 11 mm·s^{-1}, and WFR = 10 mm·s^{-1} (see online version for colours)

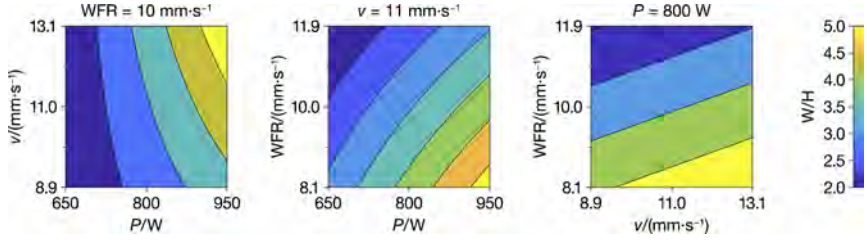

5.2 H/D analysis

The reduced model yielded an S of 1.1, an R^2(adj.) of 93%, and an R^2(pred.) of 89%, indicating highly satisfactory outcomes. The Grubbs' test identified one outlier (tests 17). As demonstrated in Table 11, only the three main effects and two-way interactions are statistically significant and have been incorporated into the model. Notably, the derived model displays no lack-of-fit or curvature, and a thorough analysis of the residuals reveals no significant concerns. Additionally, exploiting the Anderson-Darling test, the assumption of normal distribution of the residuals could not be rejected at a 5% significance level.

The regression parameters and their details are reported in Table 12. Moreover, the regression equation in coded terms is as follows:

$$H / D = 6.945 - 3.316 \cdot P - 0.727 \cdot v + 1.593 \cdot WFR - 0.857 \cdot P \cdot WFR$$

Table 11 H/D ANOVA for the reduced model

Source	*df*	*Adj. SS*	*Adj. MS*	*F*	*p-value/%*
Model	4	351.017	87.754	71.30	< 0.1
Linear	3	333.398	111.133	90.30	< 0.1
P	1	263.893	263.893	214.41	< 0.1
v	1	12.686	12.686	10.31	0.4
WFR	1	56.819	56.819	46.17	< 0.1
2-way interaction	1	17.619	17.619	14.32	0.1
P · WFR	1	17.619	17.619	14.32	0.1
Error	22	27.077	1.231		
Curvature	1	0.500	0.500	0.40	53.6
Lack-of-fit	3	2.065	0.688	0.51	68.3
Pure error	18	24.511	1.362		
Total	26	378.094			

Table 12 Estimates of H/D parameters of the model in coded units

Variable	*Parameter*	*Coef*	*SE Coef*	*p-value/%*
Constant	β_0	6.945	0.214	< 0.1
P	β_1	–3.316	0.226	< 0.1
v	β_2	–0.727	0.226	0.4
WFR	β_3	1.539	0.226	< 0.1
P · WFR	β_{13}	–0.857	0.226	0.1

Figure 15 *H/D* main effects factorial plot (see online version for colours)

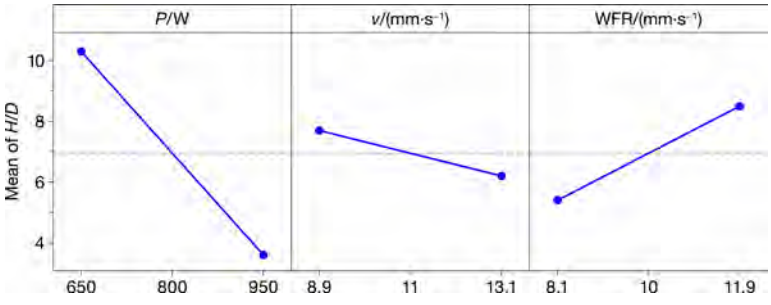

The main effects analysis, plotted in Figure 15, indicates *P* as the dominant factor in the *H*/*D* response. Specifically, an increase of *P* or *v* leads to a decrease in *H*/*D*, a finding that confirmed the results depicted in Figure 11 of Section 4.3. The latter suggests that an increase in *P* or *v*, with WFR being constant, corresponds to a simultaneous decrease in *H* and an increase in *D*. When the *v* changes, the total amount of melt material remain constant, due to constant power. However, when the v increases, most portion of the melt material is within the substrate and less out of it. Regarding the WFR main effect, which stands as the second most significant factor in this model, it can be seen that as the

amount of material fed to the melt pool increases, the *H*/*D* ratio also increases, implying an increase in *H* and a decrease in *D*.

Figure 16 *H*/*D* interaction plot (see online version for colours)

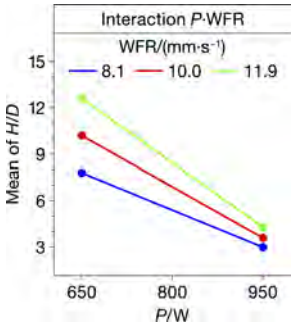

The two-way interactions involving *P* as a factor demonstrate enhanced track penetration for *P* high level, as outlined in Figure 16, corroborating the findings discussed in previous sections.

Finally, contour plots were plotted in Figure 17 in the central point.

Figure 17 *H*/*D* contour plots at *P* = 800 W, *v* = 11 mm·s^{-1}, and WFR = 10 mm·s^{-1} (see online version for colours)

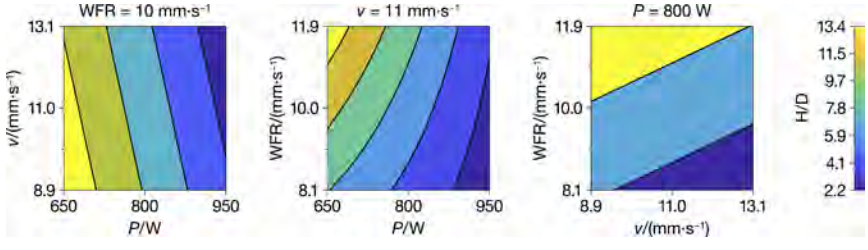

By examining the effect of process variables on the two examined ratios for the AISI 316L material deposited on AISI 304 alloy which presents almost identical thermomechanical properties the following set of parameters have been characterised as acceptable based on the *H*/*D* and *W*/*H* ratios (Jiayun et al., 2021; Wang and Kashaev, 2022). The stand-off distance is always at 6 mm as presented at the end of Section 2.

Table 13 Accepted values for process parameters

P/W	*v/(mm·s^{-1})*	*WFR/(mm·s^{-1})*
950	13.1	11.9
950	13.1	13.1
900	11.0	11.0
900	12.4	11.3
800	11.0	10.0

6 Conclusions

This comprehensive investigation, structured in two distinct phases, contributes to the existing knowledge of the wire DED-LB/M process applied to AISI 316L deposited on AISI 304 stainless steel substrates. Primarily, the effects of escalating material deposition into the melt pool are scrutinised. A qualitative assessment of the laser power (*P*) influence concerning linear energy density (*E*) is undertaken. Lastly, the impact of P is evaluated while holding the relative speed between the robotic arm and the material constant. The key output of the first phase was the understanding of the change of dimensions when the process inputs change. Additionally, throughout this work, *P*, *v*, and WFR were established as key parameters of the wire DED-LB/M process.

Subsequently, the final experimental investigation conducted through a factorial design methodology yielded a nuanced comprehension of the intricate interplay between various parameters and their consequent effects on track geometry. In this phase the evaluation considers also the ratios of *W*/*H* and *H*/*D* which determine which set of variables provide satisfied results in terms of penetration depth and can be further used in following experiments. Particular emphasis was placed on harnessing RSM techniques, coupled with ANOVA and stepwise optimisation methods. These strategies enabled the derivation of reduced models that effectively explain the observed phenomena, underscoring the power of these combined methodologies in intricate experimental analysis. The most notable finding reported by the authors are:

- The significant influence of the *P* level on the depth of the track in the substrate and on the achieved track width.
- The influence of WFR on the achieved track height.
- The critical role of *P* in manipulating and controlling the achieved penetration and of WFR on controlling the layer height, emphasising its paramount importance in the experimental model.

This investigation broadens the understanding of the wire DED-LB/M process and provides a basis for enhanced control mechanisms, thereby facilitating its broader application in diverse industrial settings. While this study presents an extensive exploration of the process parameter window, it also accentuates the need for further research.

Investigations into the impact of the examined key parameters on different designs (single walls, multi wall structures, massive parts, etc.) and on their structural performance will follow in a future work. The heat accumulation, the hardness, the porosity, the distortion as well as the surface quality are directly linked to the selection of process parameters and the path planning strategy. The latter will be also investigated in relation to the structural performance of the part. Moreover, since the calculation of *E* does not consider the wire feed speed, it is important to investigate other physics based metrics that consider also the supplied material in order to depict the influence of parameters on the track dimensions and the process stability. In conclusion, developing a predictive model for the wire DED-LB/M process, built on the findings of this and other investigations, would constitute a pivotal advancement in applying this technology within the industry.

Acknowledgements

This research has been partially supported from the European Union's Horizon Europe research and innovation program under grant agreement No. 101091869 (EU Project R3GROUP).

P. Stavropoulos has contributed to conceptualisation; H. Bikas has contributed to investigation, N. Porevopoulos has contributed to experiments; P. Stavropoulos and K. Tzimanis have contributed to methodology, writing – original draft; A. Pilagatti has contributed to analysis and writing; E. Atzeni and P. Stavropoulos have contributed to formal analysis, writing – review and editing; A. Salmi, L. Iuliano and P. Stavropoulos have contributed to visualisation, writing and review and editing.

References

Akritas, M.G. and Papadatos, N. (2004) 'Heteroscedastic one-way ANOVA and lack-of-fit tests', *Journal of the American Statistical Association*, Vol. 99, No. 466, pp.368–382.

Barnett, V. and Lewis, T. (1994) *Outliers in Statistical Data*, Vol. 3, Wiley, New York.

Bikas, H., Stavropoulos, P. and Chryssolouris, G. (2016) 'Additive manufacturing methods and modelling approaches: a critical review', *The International Journal of Advanced Manufacturing Technology*, Vol. 83, No. 1, pp.389–405.

Chen, Z., Han, C., Gao, M., Kandukuri, S.Y. and Zhou, K. (2022) 'A review on qualification and certification for metal additive manufacturing', *Virtual Phys. Prototyp.*, Vol. 17, No. 2, pp.382–405.

Domingos, P. (1999) 'The role of Occam's razor in knowledge discovery', *Data Mining and Knowledge Discovery*, Vol. 3, No. 4, pp.409–425.

Frederick, C., Bell, D. and Sonon, E. (1976) 'Improved metallographic etching techniques for stainless steel and for stainless steel to carbon steel weldments', *Metallography*, Vol. 9, No. 2, pp.91–107, ISSN 0026-0800, https://doi.org/10.1016/0026-0800(76)90008-2.

Jiayun, S., Gang, Y., Xiuli, H., Shaoxia, L., Zixun, L. and Wang, X. (2021) 'Process maps and optimal processing windows based on three-dimensional morphological characteristics in laser directed energy deposition of Ni-based alloy', *Optics & Laser Technology*, Vol. 142, p.107162, ISSN: 0030-3992, https://doi.org/10.1016/j.optlastec.2021.107162.

Lenth, R.V. (2001) 'Some practical guidelines for effective sample size determination', *The American Statistician*, Vol. 55, No. 3, pp.187–193.

Mazzarisi, M. et al. (2020) 'Phenomenological modelling of direct laser metal deposition for single tracks', *International Journal of Advanced Manufacturing Technology*, Vol. 111, Nos. 7–8, pp.1955–1970.

Minitab, L. (2023a) *Lack-of-Fit and Lack-of-Fit Tests* [online] https://support.minitab.com/en-us/minitab/20/help-and-how-to/statistical-modeling/regression/supporting-topics/regression-models/lack-of-fit-and-lack-of-fit-tests/ (accessed 23 July 2023).

Minitab, L. (2023b) *Model Reduction* [online] https://support.minitab.com/en-us/minitab/21/help-and-how-to/statistical-modeling/regression/supporting-topics/regression-models/model-reduction/ (accessed 21 July 2023).

Montgomery, D.C. (2022) *Design and Analysis of Experiments*, 9th ed., John Wiley & Sons, USA.

Montgomery, D.C. and Runger, G.C. (2020) *Applied Statistics and Probability for Engineers*, John Wiley & Sons, USA.

Mustafa, M.T., Arif, A.F.M. and Masood, K. (2014) 'Approximate analytic solutions of transient nonlinear heat conduction with temperature-dependent thermal diffusivity', *Abstract and Applied Analysis*, Vol. 2014, No. 1, pp.1085–3375.

Nelson, L.S. (1998) 'The Anderson-Darling test for normality', *Journal of Quality Technology*, Vol. 30, No. 3, p.298.

Panagiotopoulou, V.C., Papacharalampopoulos, A. and Stavropoulos, P. (2023a) *Developing a Manufacturing Process Level Framework for Green Strategies KPIs Handling*, DOI: 10.1007/978-3-031-28839-5_112.

Panagiotopoulou, V.C., Paraskevopoulou, A. and Stavropoulos, P. (2023b) 'A framework to compute carbon emissions generated from additive manufacturing processes', in Kohl, H., Seliger, G. and Dietrich, F. (Eds.): *Manufacturing Driving Circular Economy. GCSM 2022. Lecture Notes in Mechanical Engineering*, Springer, Cham, https://doi.org/10.1007/978-3-031-28839-5_35.

Panza, L., Maddis, M.D. and Spena, P.R. (2022) 'Use of electrode displacement signals for electrode degradation assessment in resistance spot welding', *Journal of Manufacturing Processes*, Vol. 76, pp.93–105, DOI: 10.1016/j.jmapro.2022.01.060.

Pilagatti, A.N., Iuliano, L. and Salmi, A. (2023) 'The role of the carrier gas flow in the directed enegy deposition process', *X ECCOMAS Thematic Conference on Smart Structures and Materials, SMART 2023*, Patras.

Piscopo, G. and Iuliano, L. (2022) 'Current research and industrial application of laser powder directed energy deposition', *International Journal of Advanced Manufacturing Technology*, Vol. 119, Nos. 11–12, pp.6893–6917, DOI: 10.1007/s00170-021-08596-w.

Piscopo, G., Atzeni, E. and Salmi, A. (2019) 'A hybrid modeling of the physics-driven evolution of material addition and track generation in laser powder directed energy deposition', *Materials*, Art. No. 2819, Vol. 12, No. 7, DOI: 10.3390/ma12172819.

Rey, P., Prieto, C., González, C., Tzimanis, K., Souflas, T., Stavropoulos, P., Rathore, J.S., Bergeaud, V., Vienne, C. and Bredif, P. (2022) 'Data analysis to asses part quality in DED-LB/M based on in-situ process monitoring', *12th CIRP Conference on Photonic Technologies [LANE 2022]*, Fürth, Germany, 4–8 September, Vol. 111, pp.345–350.

Sawilowsky, S.S. (2009) 'New effect size rules of thumb', *Journal of Modern Applied Statistical Methods*, Vol. 8, No. 2, p.26.

Sofia, J. and Ethiraj, N. (2020) *Additive Manufacturing: Past Present and Future* [online] https://ijrar.org/papers/IJRAR1BQP021.pdf (accessed 5 August 2023).

Stavropoulos, P. (2022) 'Digitization of manufacturing processes: from sensing to twining', *Technologies*, Vol. 10, p.98, https://doi.org/10.3390/technologies10050098.

Stavropoulos, P. (2023) 'AM applications', in *Additive Manufacturing: Design, Processes and Applications. SpringerBriefs in Applied Sciences and Technology*, Springer, Cham, https://doi.org/10.1007/978-3-031-33793-2_4.

Stavropoulos, P. and Foteinopoulos, P. (2018) 'Modelling of additive manufacturing processes: a review and classification', *Manufacturing Review*, Vol. 5, No. 2, pp.8–34.

Stavropoulos, P. and Panagiotopoulou, V.C. (2022) 'Carbon footprint of manufacturing processes: conventional vs. non-conventional', *Processes*, Vol. 10, p.1858, https://doi.org/10.3390/pr10091858.

Stavropoulos, P., Bikas, H., Avram, O., Valente, A. and Chryssolouris, G. (2020) 'Hybrid subtractive-additive manufacturing processes for high value-added metal components', *The International Journal of Advanced Manufacturing Technology*, Vol. 111, No. 3, pp.645–655.

Stavropoulos, P., Foteinopoulos, P., Papacharalampopoulos, A. and Bikas, H. (2018) 'Addressing the challenges for the industrial application of additive manufacturing: towards a hybrid solution', *International Journal of Lightweight Materials and Manufacture*, Vol. 1, No. 3, pp.157–168.

Stavropoulos, P., Bikas, H., Souflas, T., Tzimanis, K., Papaioanou, C. and Porevopoulos, N. (2023a) 'Chapter 29-additive manufacturing in the automotive industry', in *3D Printing: Fundamentals to Emerging Applications*, 1st ed., CRC Press, Boca Raton, https://doi.org/10.1201/9781003296676.

Stavropoulos, P., Foteinopoulos, P., Stavridis, J. and Bikas, H. (2023b) 'Increasing the industrial uptake of additive manufacturing processes: a training framework', *Advances in Industrial and Manufacturing Engineering*, Vol. 6, p.100110, ISSN 2666-9129, https://doi.org/10.1016/j.aime.2022.100110.

Stavropoulos, P., Pastras, G., Souflas, T., Tzimanis, K. and Bikas, H. (2022) 'A computationally efficient multi-scale thermal modelling approach for PBF-LB/M based on the enthalpy method', *Metals*, Vol. 12, No. 11, p.1853, https://doi.org/10.3390/met12111853.

Steinhilper, R. (1998) *Remanufacturing: The Ultimate Form of Recycling*, Fraunhofer-IRB-Verlag, Stuttgart, Germany.

Wang, M. and Kashaev, N. (2022) 'Investigation of process window for AA7075 considering effects of different wire feed directions in lateral laser metal deposition', *Procedia CIRP*, Vol. 111, pp.218–223, DOI: 10.1016/j.procir.2022.08.053.

Wohlers Report (2023) *Reports* [online] https://wohlersassociates.com/product/wr2023 (accessed 24 August 2023).

Wohlers, T., Campbell, I., Diegel, O., Kowen, J. and Huff, R. (2019) *Wohlers Report 2019*, Wohlers Associates Inc., Fort Collins.

Zuo, L, Shang, S., Xu, M., Hua, T., Chongliang, Z., Guijun, B., Adam, T., Andres, G. and Jing, C. (2022) 'High deposition rate powder-and wire-based laser directed energy deposition of metallic materials: a review', *International Journal of Machine Tools and Manufacture*, Vol. 181, p.103942, ISSN 0890-6955, https://doi.org/10.1016/j.ijmachtools.2022.103942.

Notes

1 Assuming a Type B uncertainty with a rectangular distribution as suggested by the GUM.